Continuous Separation of Microparticles in an Inertial-Based Dielectrophoretic Device

Bagheri, Narges; Ahmadi Nadooshan, Afshin**+; Bayareh, Morteza
Engineering Faculty, Shahrekord University, Shahrekord, I.R. IRAN

ABSTRACT: *In this study, polystyrene particles with different diameters suspended in deionized water are continuously separated in a novel spiral microfluidic chip using the dielectrophoretic force. The proposed device consists of two curved and straight microchannels. Deionized water and three polystyrene particles with diameters of 10, 15, and 17 μm enter the microchannel. In the curved part, the larger particles are separated from the 10-μm particles due to inertial force. An array of three planar microelectrodes is located on the bottom wall of the straight section. By applying an alternating current to the microelectrodes, a non-uniform electric field is created to separate larger particles (15- and 17-μm ones). Various simulations are performed at Reynolds numbers (Re) from 50 to 150. For Re = 100, 15- and 17-μm particles are completely separated from 10-μm particles. The results demonstrate that at a voltage of 80-100 V, 17-μm particles are separated from 15-μm particles due to negative dielectrophoresis. In addition, increasing the electrical voltage enhances the distance of the 17-μm particle flow from the 15-μm particle flow.*

KEYWORDS: *Microfluidic; Inertial separation; Spiral microchannel; Dielectrophoresis; Microelectrode.*

INTRODUCTION

Microfluidic technology is the science of designing and studying micro-devices that can analyze small amounts of liquids [1, 2]. Microfluidic technology has many applications such as biological and chemical reactions, and isolation and diagnostic processes using microchips [3]. Significant advantages of this technique over conventional technologies are small sample size, rapid sample processing, high sensitivity and accuracy, low cost, portability, etc. [4]. One of the main applications of microfluidic technology is the development of lab-on-chip and point-of-care devices [5]. This technology also has great potential for applications in biology, chemistry, medicine, mixing, drug delivery, drug synthesis and screening, monitoring of environmental activities, detection of biological reagents, and study of cellular processes [1]. One of the most important applications of microfluidic technology is the manipulation and separation of cells and particles (synthetic and biological). The particle separation process is of great importance in the fields of medicine, biology, chemistry, the food industry, and the environment [6]. The flow regime in microfluidic devices is usually laminar, which allows precise flow control and prediction. Microfluidic particle separation can be performed using three ways [6]: i) Passive methods that are based on microchannel geometry, the existence of various obstacles in the flow direction, and

* *To whom correspondence should be addressed.*
+ E-mail: ahmadi@sku.ac.ir
1021-9986/2023/7/2260-2274 *15/$/6.05*

interaction between particles and geometry. Microfiltration [7] and Deterministic Lateral Displacement (DLD) [8] by placing obstacles and also inertial separation [9] are two common methods of passive separation of microparticles. The structure of microchannel geometry in the passive separation method is usually complex. ii) Active methods that are based on the use of an external field. In these methods, the structure of microchannel geometry is simple. Isolation using electric [10], magnetic [11], acoustic [12] and optical [13] fields are common methods of active microfluidic separation. iii) The hybrid methods that use active and passive methods simultaneously.

When a neutral particle suspended in a fluid is exposed to a non-uniform external electric field, a force is applied to the particle from the external field that causes it to move laterally. This phenomenon is called dielectrophoresis [14]. When a particle is exposed to an electric field, the internal electrical charges of the particle and the suspension medium (the medium in which the particle is suspended) accumulate on the interface of the particle and the medium, and induced electric dipoles are formed on the interface [15]. If the electric field is uniform, the charge density is the same on both sides of the particle, and as a result, the magnitudes of the induced dipoles are equal. Therefore, the resultant of the forces exerted by the field on the particle is equal to zero and the particle does not move. However, if the electric field is non-uniform, the magnitude of the induced dipoles on both sides of the particle is unequal, and as the particle becomes polarized and oriented in the direction of the field vectors, the dielectrophoretic force is applied to the particle. The unique feature of dielectrophoresis is that it can be applied to both neutral and charged particles [15]. The amount of dielectrophoretic force depends on three general parameters: i) particle properties such as dielectric properties of the particle and its shape and size (diameter), ii) properties of suspension medium such as permeability and electrical conductivity, and iii) electric field gradient. Accordingly, the stronger the applied electric field, the larger the particle diameter, and the greater the difference between the particle's electrical conductivity and permittivity and the medium, the greater the dielectrophoretic force generated [14]. This method has many applications in medical, biological, clinical, and environmental fields. This method is used to concentrate, isolate and control the movement of various biological particles, including cells, microorganisms, bacteria, and viruses [14, 15].

One of the most widely used passive methods is the separation by inertial forces. In this method, the inertial forces due to the intrinsic properties of the fluid flow and the shape of the microchannel force the particles to move across the microchannel (depending on the particle size) and in a specific transverse position to reach equilibrium [16]. The inertial force exerted on the particles consists of two main forces: the wall repulsion force and the force due to the fluid shear gradient. In curved channels, the fluid flows along the outer wall of the channel travels a greater distance than the fluid flows along the inner wall of the channel. Hence, the velocity of the fluid near the inner wall is higher, but to maintain the fluid continuity, a secondary flow is created from the inner walls toward the outer wall, resulting in the formation of two symmetrical vortices that are known as Dean vortices. Particles located along these vortices rotate with them until an inertial force overcomes them and reaches a spatial equilibrium across the channel [17, 18].

In the last two decades, many studies have been performed experimentally and numerically in the field of the dielectrophoretic separation of cells and biological particles. *Pammer et al*. [19] separated platelets from red blood cells using a two-stage microfluidic device with a voltage of 100 V and a frequency of 1 MHz. *Piacentini et al*. [20] used a microfluidic device to separate platelets with a purity of 98.8% from red blood cells using a negative dielectrophoretic force. *Jing et al*. [21] isolated intestinal cancer cells and white blood cells and reached efficiencies of 82% and 92%, respectively. The sample flow rate was 0.3 ml/hour and the frequency and voltage of the electric field were reported to be 100 kHz and 5 V, respectively. *Kumar et al*. [22] proposed a three-dimensional model to show the isolation of intestinal and E-coli bacteria from blood cells when the voltage and frequency of the electric field were 19.5 V and 100 kHz, respectively.

Polystyrene particles have been widely used in experimental studies due to their stable physical and chemical properties to perform numerical simulations to predict and optimize the microfluidic system. Numerous studies have been performed numerically and experimentally on the isolation of polystyrene

particles suspended in water. In an experimental and numerical study, *Boyung et al*. [23] separated 3- and 10-μm polystyrene particles in a continuous flow of deionized water.

Inertial separation was first proposed in 1961 by Segre and Silberberg [24]. During an experiment on particles suspended in a fluid flow inside a 1-cm channel, they observed that the particles migrate laterally after a short distance from the channel inlet and reach an equilibrium position equal to 0.6 of the channel radius. On a micro-scale, research in this area began with revolutionary work by *DiCarlo et al*. [25] in 2007. They used an innovative geometry called a serpentine channel to focus polystyrene microparticles suspended in water. Many researchers have employed inertial effects to separate particles and cells. For example, *Shiriny* and *Bayareh* [18] by adjusting the flow rate of sample flow and buffer flow separated two types of cancer circulating cells in the bloodstream from white and red blood cells (with diameters of 8-10 microns) using the inertial separation mechanism in a single-loop spiral channel. They reported that the flow rate of fluid (blood plasma diluted with phosphate solution) to achieve 100% separation efficiency and purity in the proposed microchannel should be in the range of 113-139 ml/min.

In the present study, a three-dimensional microchannel is designed and proposed using to isolate polystyrene microparticles using a combination of inertial separation and dielectrophoretic focusing. The proposed device consists of two curved and straight microchannels. Three polystyrene particles with diameters of 10, 15 and 17 μm enter the designed microchannel with a stream of deionized water. An array of three plate microelectrodes is located on the bottom wall of the straight section of the microchip. By applying an alternating current to the microelectrodes, a non-uniform electric field is created in the straight part. As a result, the dielectrophoretic force is applied to the particles. COMSOL Multiphysics software 5.6 is employed to perform simulations. The effect of Reynolds number and voltage applied to the electrodes on the efficiency and purity of separation is investigated.

THEORETICAL SECTION

Microchannel geometry

The proposed microchannel consists of three parts: the curved section, the divergent channel, and the straight rectangular section. The curved part is a 270-cm circular segment with a curvature radius of 1 cm and a width of 500 μm located at the beginning of the microchannel. There are two inlets at the beginning of the curved section so that the width of the internal and external ones is 350 and 150 μm, respectively. The purpose of the inlet design is to inject sample streams, including fluid with microparticles, from the external inlet and buffer flow, consisting of fluid without particles, from the internal inlet to focus the particles [26] at the channel inlet. The height of this section is 200 μm. Particle inertial separation takes place in this part of the microchannel. The rectangular part is designed to separate the particles due to the dielectrophoretic effect. The length and width of this part are 19 and 2.5 mm, respectively. An array of three planar microelectrodes is placed in this section. The height of this part is 200 μm. A negative voltage is applied to the rectangular electrodes and a positive voltage is applied to the middle electrode.

Governing gquations

Investigation of the two-phase flow within the microchannel is performed using an Eulerian-Lagrangian approach. In this model, the fluid is first considered as a continuous single-phase and the governing equations are solved in the Eulerian framework. The motion of the particles is then modeled using the Lagrangian model, which considers the particle as a discrete phase. It should be noted that the motion of the particles is affected by the continuous phase (fluid) but the flow of the fluid is not affected by the motion of the particles. As a result, a one-way coupling is established here. The governing equations of the problem can be divided into three categories: fluid flow, electric field, and particles. The Reynolds number is introduced as follows to determine the fluid flow regime:

$$Re=\frac{\rho U_{avg} D_h}{\mu} \quad (1)$$

where $D_h=2wH/(w+H)$ is channel hydraulic diameter. ρ and μ are the density and viscosity of the fluid, U_{avg} is the average velocity of the fluid, w is the width of the channel and H is its height. Since the Reynolds number varies in the range of 50-150, the flow regime is laminar (Stokes flow) [27]. The equations governing the continuous flow of incompressible and Newtonian fluids are continuity and momentum equations. The continuity equation is:

$$\nabla.V=0 \quad (2)$$

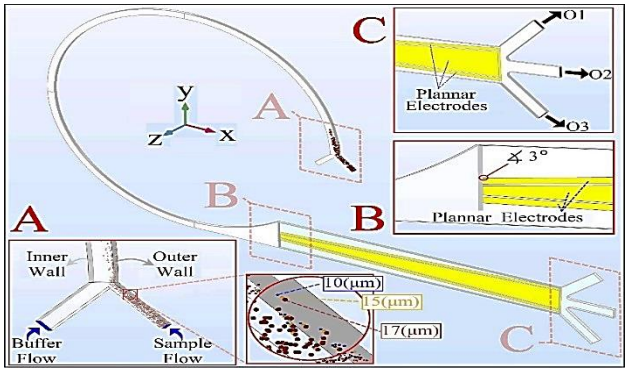

Fig. 1: Proposed microchannel geometry

Here, V is the fluid velocity vector. The momentum equation is:

$$\rho(\vec{V}.\nabla)\vec{V}=-\nabla P+\mu\nabla^2\vec{V} \quad (3)$$

Where P represents pressure. As mentioned before, the curvature of the microchannel causes the formation of Dean vortices in the transverse section. The magnitude of these vortices is determined by the Dean number [9]:

$$De=Re\sqrt{\frac{D_h}{2R}} \quad (4)$$

Where R is the radius of curvature of the channel. The velocity of the secondary flow called the Dean flow is as follows [28]:

$$U_{Dean}=1.8\times10^{-4}\ De^{1.63} \quad (m/s) \quad (5)$$

The governing equation of electric current according to Ohm's law by neglecting inductive effects is [29]:

$$\nabla.J=0 \quad (6)$$

$$J=\sigma_m E+j\omega D \quad (7)$$

$$D=\varepsilon_0\varepsilon_m E \quad (8)$$

$$E=-\nabla.V \quad (9)$$

where D is the electric displacement and E is the electric field strength. Also, j is an imaginary, σ_m and ε_m are the electrical conductivity and the electrical permeability of the fluid, respectively. $\varepsilon_0=854.8\times10^{-12}$ (F/m) is the electrical permeability of the vacuum. In addition, $\omega=2\pi f$, where ω is the field angular frequency and f is the electric current frequency. The relationship of electric current conservation can be written from the combination of Eqs. (6-9) as follows [29]:

$$\nabla^2V=0 \quad (10)$$

The general equation governing the particle motion is derived from Newton's second law:

$$\frac{d}{dt}(m_P v)=F_{tot}=F_D+F_L+F_{DEP} \quad (11)$$

Here, m_P and v are the mass and velocity of the particles and F_{tot} id the result of external forces applied to particles, including drag force, F_D, inertial lift force, F_L, and electrophoretic force, F_{DEP}. It should be noted that the gravitational force can be neglected due to the proximity of the density of particles and fluids. The Brownian force is also important when the particle is of nanoscale. Therefore, considering the micron diameter of the particles, the amount of the Brownian force is negligible compared to other forces.

Since the fluid flow regime is in the Stokes flow regime, F_D is [30]:

$$F_D=\frac{1}{\tau_P}m_P(u-v)f_D \quad (12)$$

$$\tau_P=\frac{\rho_p d_p^{\,2}}{18\mu} \quad (13)$$

Where $f_D=\left[1-\frac{9}{16}\alpha+\frac{1}{8}\alpha^3-\frac{45}{256}\alpha^4-\frac{11}{16}\alpha^5\right]^{-1}$ is drag correction coefficient due to the effect of microchannel walls, $\alpha=\frac{r_p}{r_p+L}$, where r_p and L are the radius of particles and the distance of the microparticles to the nearest wall, respectively [18]. It should be noted that in the direction of the secondary flow, the drag force applied to the particles is called Dean drag and is $F_D=6\pi r_p\,\mu U_{Dean}$ [17]. The inertial lift force is [9]:

$$F_L=\frac{\rho U_{max}^{\,2} d_p^{\,4}}{D_h^{\,2}}f_L \quad (14)$$

Where f_L is the lift force coefficient that is a function of the channel Reynolds number $Re_C=\frac{\rho U_{max} D_h}{\mu}$ and the position of the particle across the channel width [17], where the maximum fluid velocity is $U_{max}=2U_{avg}$ [9]. The dielectrophoretic force is obtained as follows [31]:

$$F_{DEP}=2\pi\varepsilon_0 r_p^{\,3}\,Real(\varepsilon_m)\,Real(CM)\nabla|E|^2 \quad (15)$$

$$CM=\frac{\varepsilon_P^*-\varepsilon_m^*}{\varepsilon_P^*+2\varepsilon_m^*} \quad (16)$$

Here, ε_P^* and ε_m^* are the complex electrical permeability of the particle and the medium, respectively, and are defined as follows:

$$\varepsilon_P^*=\varepsilon_0\varepsilon_m-j(\sigma_P/\omega) \quad (17)$$

$$\varepsilon_m^*=\varepsilon_0\varepsilon_m-j(\sigma_m/\omega) \quad (18)$$

Where σ_P is the electrical permeability of the particle that is as follows for solid and homogeneous spherical particles [32]:

$$\sigma_P=\frac{2K_s}{r_P} \quad (19)$$

Here, K_s is the particle surface conductance.

Numerical simulation

The discretization of the momentum equations is set to P2+P1; Thus, in the numerical solution of the above equations, the calculations are performed for the velocity field up to the second-order derivatives and for the pressure field up to the first-order derivatives, and the higher-order derivatives for each field are omitted. The no-slip boundary condition is imposed on the microchannel walls and the zero gauge pressure condition is established at the outlets. The insulation electrical boundary condition is applied to the channel walls and negative and positive voltages are applied to rectangular and trapezoidal electrodes, respectively. In this study, the current frequency is set to 100 kHz and different voltage values equal to 50-100 V are considered. Particle motion modeling is done using a particle tracing module. 80 particles with a diameter of 10 μm, 80 particles with a diameter of 15 μm, and 80 particles with a diameter of 17 μm are injected into the channel at a velocity equal to the inlet velocity of the fluid flow. The solution is transient with a convergence criterion of 10^{-5}. Table 1 presents the physical properties of fluid and particles. In this table, $\sigma_{m,1}$, $\sigma_{m,2}$, and $\sigma_{m,3}$ are electrical conductivity of 10-, 15-, and 17-μm particles.

Validation

To ensure numerical solution, dielectrophoretic and inertial separation methods are verified separately with experimental results. First, the work of *Chen et al*. [3] is modeled using COMSOL Multiphysics software and the obtained results are compared with the experimental results. A rectangular microchannel with length, width, and height of 800, 200, and 50 μm, respectively, is considered. Two inlets with widths of 100 μm and an angle of 30° are placed to inject liquid flow containing particles and buffer flow. The 5-, 10-, and 20-μm polystyrene particles with a flow rate of 3 μL/min are injected into the channel. Four electrodes with a width of 200 μm are placed at a distance of 200 μm on the bottom wall of the channel. The voltage applied to the electrodes is ± 10 V and the electric field frequency is set to 1 MHz. A view of the particle motion path is shown in Fig. 2B. Also, the location of the particles along the channel obtained from the present simulations is shown in Fig. 2C. The agreement between the simulation results and the reference experimental data indicates the accuracy of the numerical solution method.

Table 1: Physical properties of fluid and particles used in the present study [32]

Parameter	Value
ρ	1000 (kg/m^3)
μ	0.001 (Pa.s)
ε_m	78
σ_m	0.2 (mS/m)
ρ_P	1050 (kg/m^3)
ε_P	2.5
K_s	1 (nS)
$\sigma_{m,1}$	0.4 (mS/m)
$\sigma_{m,2}$	0.267 (mS/m)
$\sigma_{m,3}$	0.235 (mS/m)

To ensure the numerical solution method of inertial separation, the experimental research of *Bhagat et al*. [9] is used. A spiral microchannel with 5 loops and a rectangular cross-section with length and width of 100 and 50 μm, respectively, consisting of two inlets and two outputs are considered. The first loop radius of the channel is 3 mm and the distance between the two consecutive loops is 250 μm. Water enters the microchannel with 50 polystyrene particles with a diameter of 1.9 μm and 50 polystyrene particles with a diameter of 7.32 μm. Buffe r flow enters from the outer inlet without particles. The inlet flow rate is 10 μL/s. The trajectory of the particles is shown in Fig. 3A. As can be seen, 7.32-μm particles (red color) migrate towards the inner wall of the channel due to the inertial force and exit from the inner outlet, separating

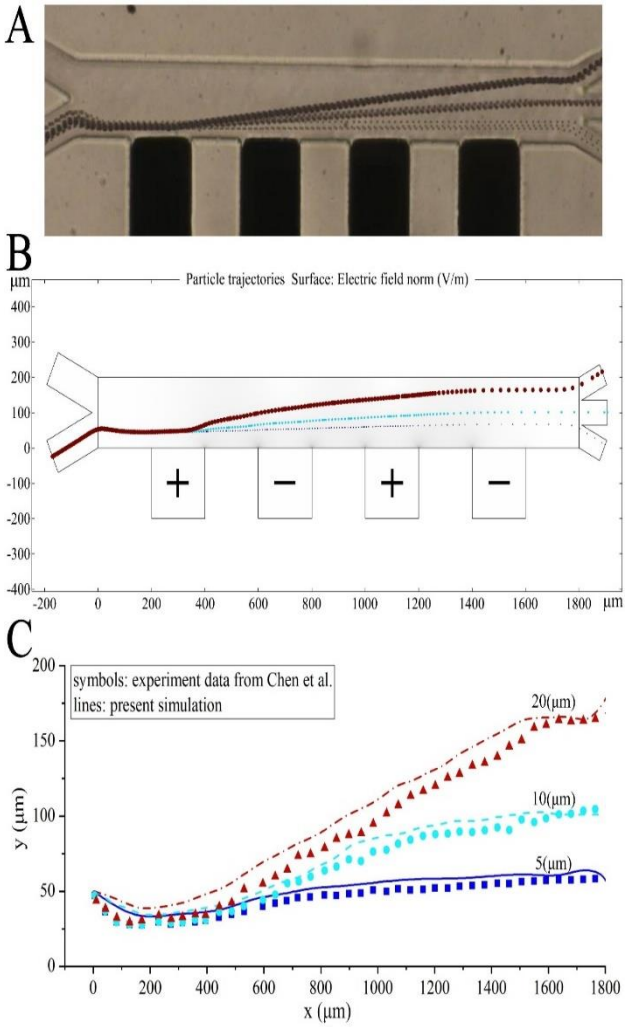

Fig. 2: (A) The particle trajectories for the experimental work of Chen et al. [3], (B) the particle trajectories obtained from the present simulations, and (C) quantitative comparison between the simulation results and experimental data

from the 1.9-μm particles (blue color). Figs. 3B and 3C show the lateral distribution of particles in the microchannel outlet reported by the reference [9] and obtained from the present numerical simulation, respectively, showing good agreement between the results.

Grid study

Grid resolution is one of the factors that strongly influence numerical simulation. Choosing the appropriate grid with optimal element size is critical to maintaining the accuracy of solving finite element problems. The present simulations are performed for Re = 100 and the electrode voltage of ± 100 V using a quadratic mesh with different element sizes and the maximum values of the fluid velocity and the electric field strength are calculated. Fig. 4 shows the electric field strength and maximum velocity in the microchannel cross-section for 5 different computational grids, indicating that the results do not change as the number of elements exceeds 4117060. Hence, the grid with 4117060 elements is selected for further simulations.

RESULTS AND DISCUSSION

As mentioned before, the fluid velocity field is first modeled steadily in the absence of particles to obtain the fluid velocity profile inside the microchannel. Fluid flow (deionized water) is injected into the proposed microfluidic device from the two inlets at different Reynolds numbers ($50 \leq Re \leq 150$). It should be noted that the ratio of different inlet flows is considered and the optimal value is obtained so that the flow rate of the internal inlet to the external one is 24 to 1. To adjust the velocity values in the microchannel inlets, the following analysis is performed:

$$Q_{tot}=Q_{Buffer}+Q_{Sample}=(24+1)Q_{Sample}=25A_{in,Sample}\times V_{Sample}$$

Here, Q represents the volume flow rate of the fluid, V is the inlet velocity, and A_{in} is the inlet cross-sectional area. $Q_{tot}=(WH)U_{avg}$ is used to calculate the volume flow rate in the microchannel. Also, the average fluid velocity is $U_{avg}=\frac{Re.\mu}{\rho D_h}$. Besides, $A_{in,Sample}=150H$. Hence, $V_{Sample}=0.47\ Re\ \left(\frac{mm}{s}\right)$ and $V_{Buffer}=4.8\ Re\ \left(\frac{mm}{s}\right)$.

The fluid velocity contours along the microchannel are shown in Fig. 5 at the plane z = 100 μm for Re = 100.

As shown in Fig. 5, the maximum velocity occurs at the channel centerline. This is more clearly shown in Fig. 6, where the velocity profile is presented in the cross-section of the curved section of the channel for Re = 100.

One of the most important factors influencing the inertial separation behavior of particles is the formation of secondary flows and Dean vortices in the cross-section of the channel. Fig. 7 shows the secondary flow velocity contours for Re = 100. The arrows shown in the Figure indicate the direction of rotation of Dean vortices.

Fig. 7 illustrates that two symmetrical vortices are formed in the upper and lower halves of the channel, and Dean velocity is maximum at the center of the channel. For a better representation, the Dean velocity profile is plotted in Fig. 8 in the microchannel center, i.e. 0.5*w*. In this Figure, the center of formation of Dean vortices, where the Dean velocity is zero, is shown on lines 58 and 148 μm.

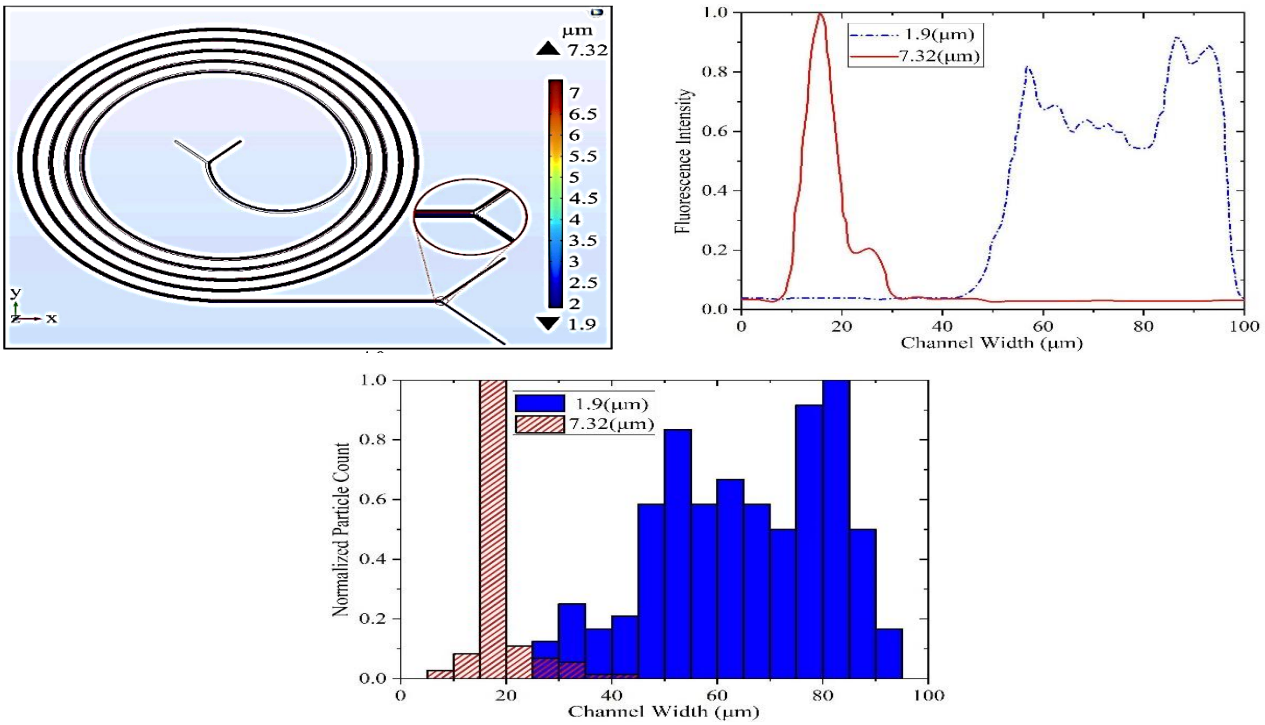

Fig. 3: (A) The trajectory of the particles achieved from the present simulation, (B) experimental results [9], and (C) present simulation results

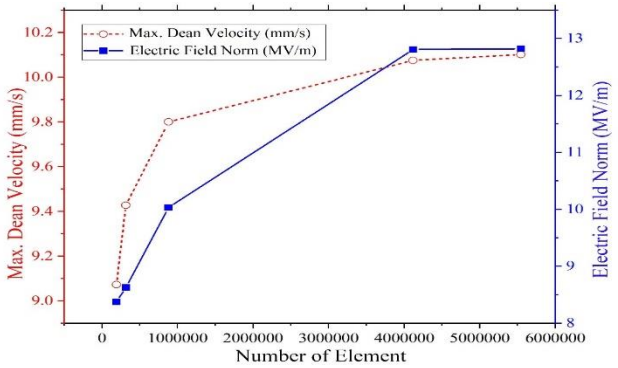

Fig. 4: Electric field strength and maximum velocity for different grid resolutions

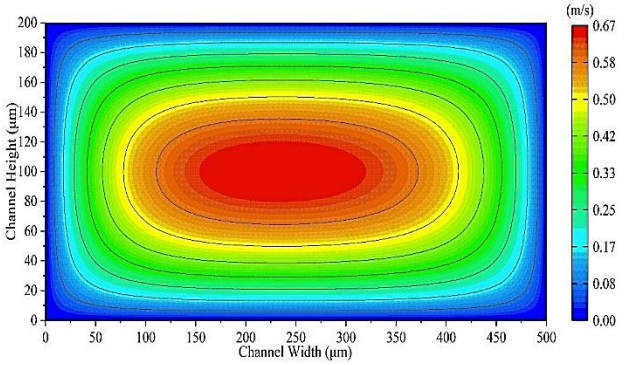

Fig. 6: The fluid velocity in a cross-section of the microchannel curve at Re = 100

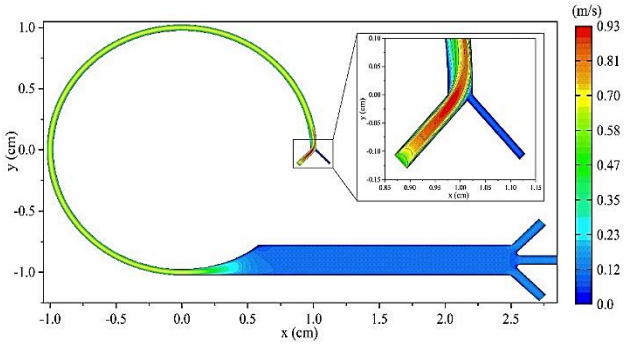

Fig. 5: Fluid velocity contours in the microchannel at Re = 100

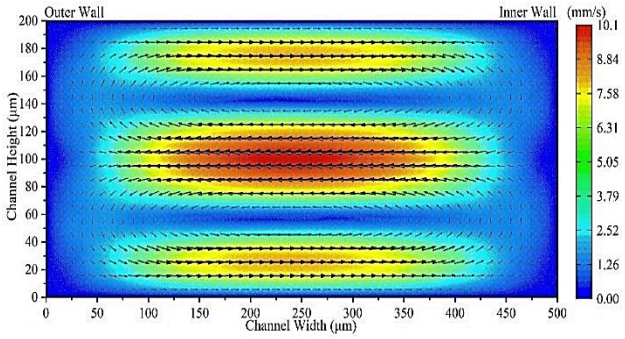

Fig. 7: Dean velocities at a cross-section of the microchannel curve at Re = 100

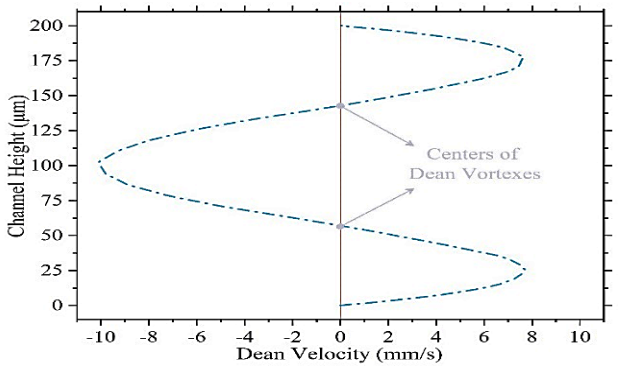

Fig. 8: The Dean velocity at the centerline of the channel cross-section for Re = 100

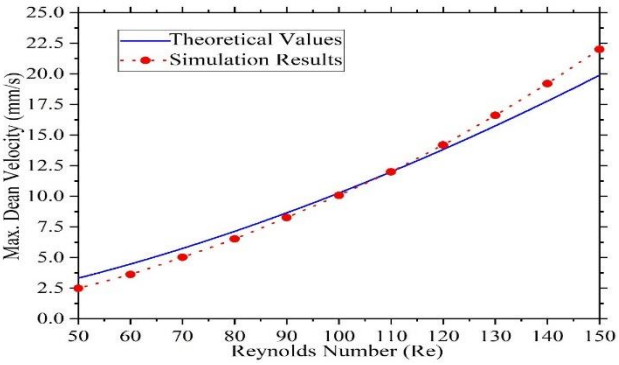

Fig. 9: The maximum Dean velocity for different Reynolds numbers calculated using Eq. 5 and obtained from the simulations

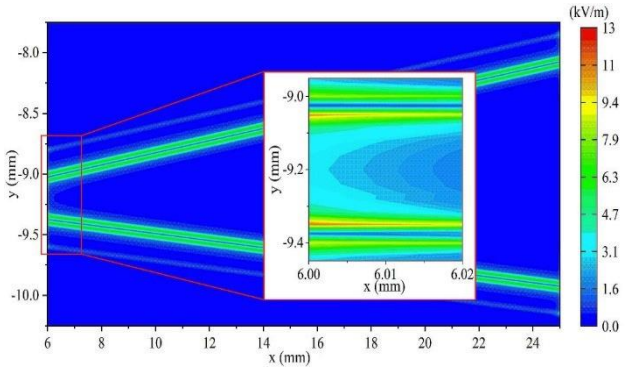

Fig. 10: The intensity of electric current in the straight section of microchannel for voltage of 100 V

The values of volume flow rate and Dean number for different Reynolds numbers used in the present simulations are presented in Table 2.

As can be seen in Table 2, as the Reynolds number increases, the Dean number and the strength of Dean vortices are enhanced. Therefore, it is expected that the Dean velocity increases with the increase of the Reynolds number. This is illustrated in Fig. 9 which shows the maximum

Table 2: Total volume flow rate and Dean number for different Reynolds numbers

Re	Q_{tot}(ml/h)	De
50	63	6.0
60	75.6	7.2
70	88.2	8.4
80	100.8	9.6
90	113.4	10.8
100	126.0	11.9
110	138.6	13.1
120	151.2	14.3
130	163.8	15.5
140	176.4	16.7
150	189.0	17.9

Dean velocity for different Reynolds numbers calculated using Eq. 5 and obtained from the simulations.

Using the steady solution of the flow field equations, the electric field distribution in different sections of the microchannel is obtained for f = 100 kHz. To examine the effect of current intensity on particle separation behavior, different values of peak-to-peak voltage, 100 V≤V_{PP}≤200 V, are employed. Fig. 10 shows the electric current intensity (E) in the straight section of the microchannel for the electrode voltage equal to ± 100 V.

The intensity of the electric field is greater along the edges of the electrodes, where electrodes with opposite electrical potentials are placed next to each other (Fig. 10). According to the results, it is expected that the effect of the electric field on particle separation to occur only in these areas because the electric field intensity is almost negligible in other regions (blue color in Fig. 10). Also, the maximum electric current intensity (E) is formed at the initial edges of the electrodes at x = 0.6 cm. By obtaining the electric field strength in the microchannel, the distribution of dielectric force on the particles can be calculated using Eq. 15. In Fig. 11, the maximum amount of dielectrophoretic force applied to the particles is presented for different voltages.

As shown in Fig. 11, the amount of dielectrophoretic force increases with the electrical voltage. The maximum force occurs at x = 0.6 cm. Since the maximum value of the electric field at the inlet of the straight part of the microchannel takes place at x = 0.6 cm, the distribution of dielectrophoretic force components on 17-μm particles is

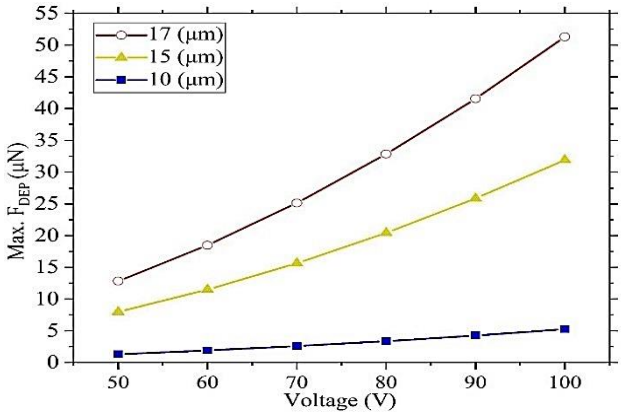

Fig. 11: The maximum dielectrophoretic force applied to the particles for different current voltages

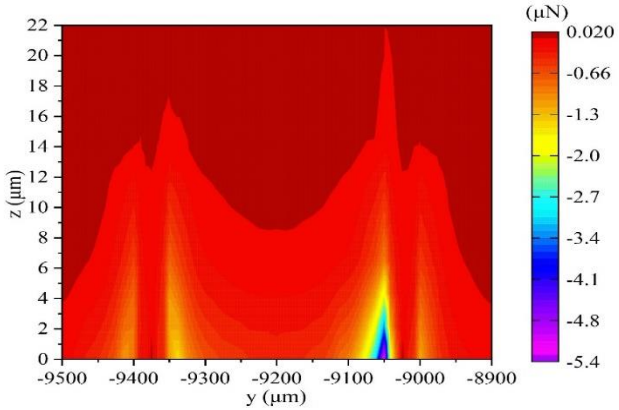

Fig. 12: The x-component contours of dielectrophoretic force applied to 17-μm particles at x = 0.6 cm for a voltage of 100 V

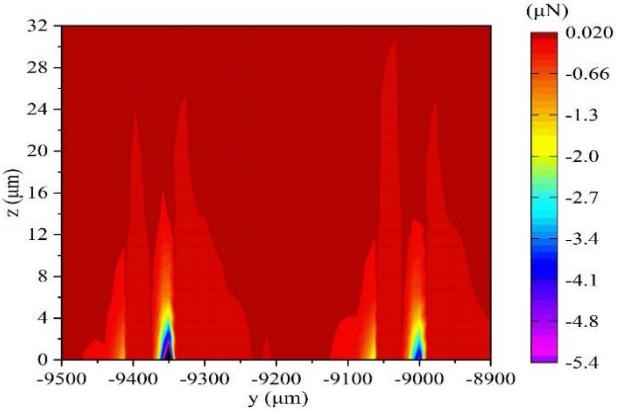

Fig. 13: The y-component contours of dielectrophoretic force applied to 17-μm particles at x = 0.6 cm for a voltage of 100 V

illustrated in Figs. 12, 13, and 14. It is confirmed that the maximum dielectrophoretic force is along the initial edges of the areas between the electrodes.

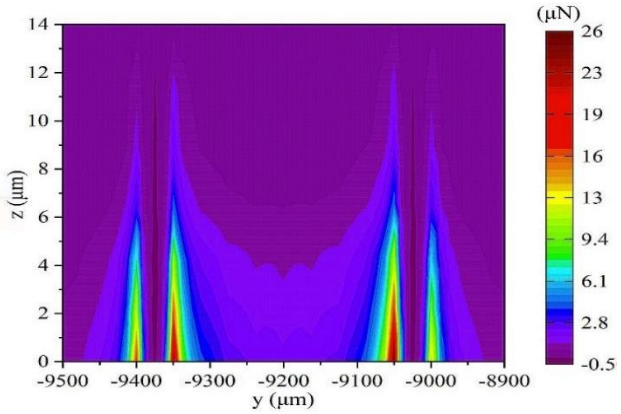

Fig. 14: The z-component contours of dielectrophoretic force applied to 17-μm particles at x = 0.6 cm for a voltage of 100 V

In this study, polystyrene microparticles (ρ = 1050 $\frac{kg}{m^3}$) with diameters of 10, 15, and 17 μm are injected into the outer inlet of the microchannel. They are separated from each other due to inertial force and Dean drag force initially. Then, by applying an electric field in the straight part of the microchannel, the complete separation of the particles occurs. According to previous experimental and numerical studies, to perform inertial separation of particles in microfluidic devices, two conditions must be provided: First, the blockage ratio of the device, (d_P/H), should be greater than 0.07. The second condition is that the particle Reynolds number, Re_P=$Re_C\left(\frac{d_P}{H}\right)^2$, should be of the order of 1 [9], where Re_C is channel Reynolds number [33]. The blockage ratio for 10-, 15-, and 17-μm particles is 0.05, 0.075, and 0.085, respectively. The maximum value of particle Reynolds number is 2.17 for 17-μm particles when Re_C = 150. It is expected that inertial separation of 15- and 17-μm particles occurs at higher Reynolds numbers, e.g. 90 and 80. Fig. 15 shows the particle trajectories for Reynolds numbers from 80 to 130 in the absence of an electric field.

As shown in Fig. 15, for 10-μm particles, the amount of drag force overcomes the inertial force and therefore the particles circulate along the Dean vortices to reach the microchannel outlet. It is expected that 15- and 17-μm particles to migrate from the outer walls of the channel to the inner wall due to inertial force at Re ≥ 90. Thus, the simulations in which smaller particles (10 μm) migrate toward the channel outlet O_3 are desirable. This can be seen for the Reynolds number of 100 in Fig. 15. To better realize particle trajectories, they are plotted in Fig. 16 for

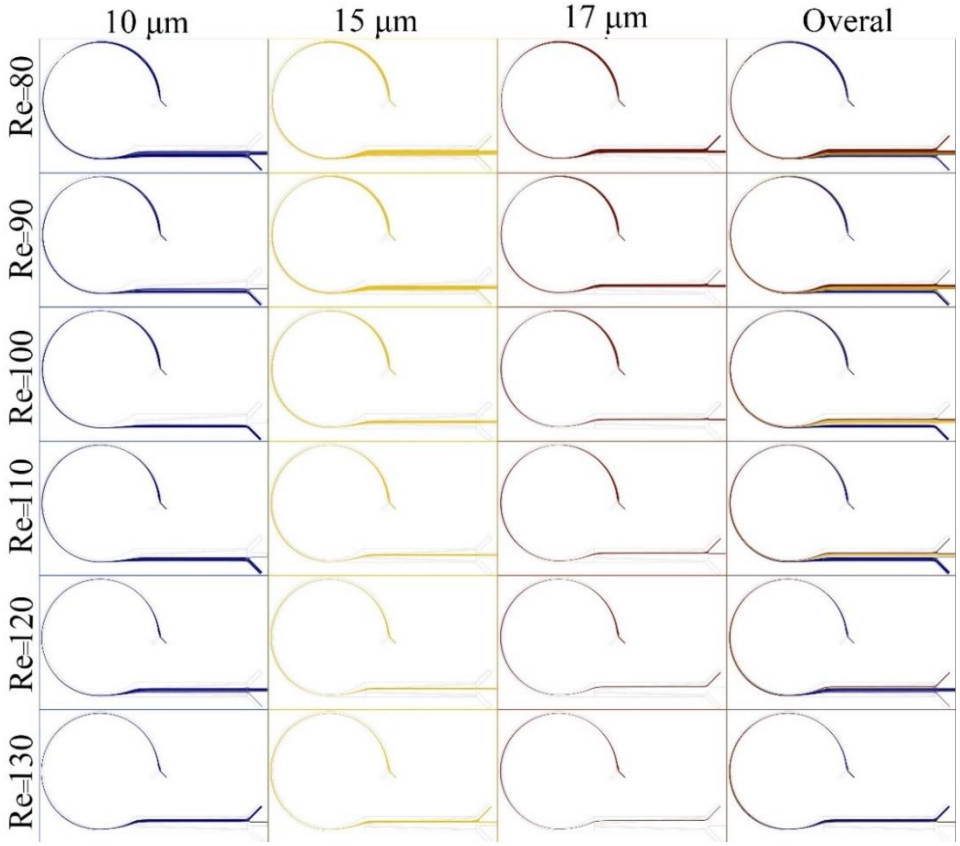

Fig. 15: Particle trajectories without applying an electric field for different Reynolds numbers

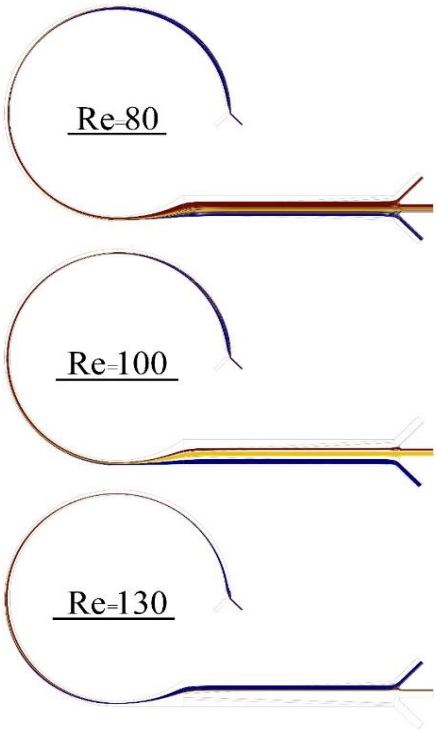

Fig. 16: Particle trajectories without applying electric field for Reynolds numbers of 80, 100, and 130

Reynolds numbers of 80, 100, and 130. At Re = 100, all 10-µm particles (blue color) pass through the outlet O_3, while 15-µm particles (yellow color) and 17-µm particles (red color) do not enter the outlet O_3. Therefore, under these conditions, 10-µm particles are completely separated from larger particles. At Re = 80, part of the 10-µm particles passes through the outlet O_3 and the rest exits from the outlet O_2 with larger particles. At Re = 130, the 10-µm particles migrate toward the inner wall of the channel and pass through outlet O_1. Therefore, the optimal separation for 10-µm particles occurs at Re = 100.So far, suitable condition for inertial separation of 10-µm particles from 15- and 17-µm particles corresponds to Reynolds numbers of $90 \leq Re \leq 110$. Now, two larger particles are separated by applying an electric field. According to the theoretical relationship proposed for the dielectrophoretic force (Eq. 15), there are two important factors in determining the amount of this force and consequently, the rate of separation is the particle diameter and Re(CM). Fig. 17 shows the variations of Re(CM) as a function of current frequency for different microparticles.

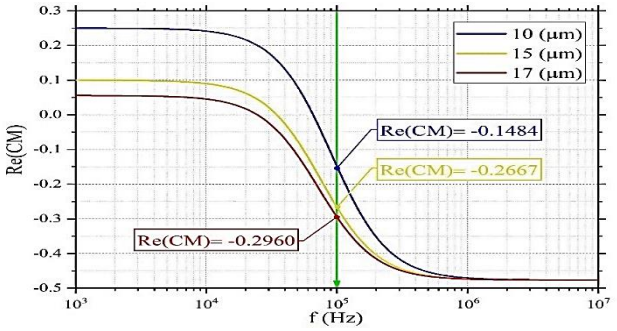

Fig. 17: The real part of the CM factor for different current frequencies

Since the frequency of 100 kHz is used to perform the present simulations, the value of Re(CM) is negative for all three particles and is equal to -0.1484, -0.2667, and -0.2960 for 10-, 15- and 17-μm particles, respectively. As a result, under the conditions described in this study, a negative dielectrophoretic force is applied to all particles and drives them away from the areas with the highest electric field strength. Fig. 18 shows the particle trajectories for different values of the voltage applied to the electrodes at Re = 100.

As can be seen in Fig. 18, the application of an electric field does not affect the trajectories of 10- and 15-μm particles along the microchannel, and only the effect on 17-μm particles is evident. Increasing the electrical voltage from 50 to 100 V enhances the dielectric force (Fig. 11). As the electrical voltage increases, the deflection of the 17-μm particles is enhanced and all particles are completely separated from each other for 80, 90, and 100 V. It should be noted that the maximum amount of dielectrophoretic force occurs at x = 0.6 cm. The spatial distribution of 10-, 15-, and 15-μm particles at the channel outlet is shown in Fig. 19 for different electrode voltages at Re = 100. As can be seen, complete separation of particles occurs at Re = 100 and an electrical voltage of 80 V.

To determine the performance of the microfluidic device and to estimate its separation capacity, separation efficiency and separation purity are defined:

$$\text{Separation efficiency} = \frac{\text{Number of specific particles exiting from outlet } O_i}{\text{Total number of particles exit from all outlets}} \times 100$$

$$\text{Separation purity} = \frac{\text{Number of specific particles exiting from outlet } O_i}{\text{Total number of particles exit from the outlet } O_i} \times 100$$

The above definitions are based on the fact that the target outlet for 10-, 15- and 17-μm particles is O_3, O_2, and O_1 (Fig. 1), respectively. Accordingly, the number of particles exited from each outlet is counted and the efficiency and purity of separation are calculated. Figs. 20 and 21 show the efficiency and purity of particle separation for different Reynolds numbers without applying an electric field, respectively.

As can be seen from Fig. 20, the separation efficiency of 100% is achieved for 10-μm particles at Re = 100. For 15- and 17-μm particles, the separation efficiency of 100% occurs at Re = 100-120, and 120-130, respectively. It is observed that only at Re = 100, complete separation of 10-μm particles occurs. The calculated values of efficiency and purity of separation by applying an electric field are presented in Figs. 22 and 23 for different values of the voltage applied to the electrodes at Re = 100. As can be seen, all particles are completely separated from each other at Re = 100 for voltage values of 80, 90, and 100 V.

CONCLUSIONS

This article examines the isolation of polystyrene particles in the continuous flow of deionized water numerically using a novel microfluidic device. To take advantage of active and passive separation methods simultaneously and improve the efficiency of the device, the design is performed so that the particles with diameters of 10, 15, and 17 μm suspending in the deionized water are separated using inertial and dielectrophoretic forces. The simulation is performed using COMSOL Multiphysics 5.6 software. The proposed microchannel consists of a curved part and a straight rectangular section. Microchannel inlets are designed to inject sample flow containing deionized water and polystyrene particles and buffer flow containing deionized water without particles. Three outlets are located at the end of the microchip. Three plane electrodes are installed at the bottom of the straight part of the channel to apply the dielectrophoretic force. The effect of inlet flow velocity and electric field intensity on the performance of the device is investigated. The results show that at Re = 100 and the voltages of 80, 90, and 100 V, the efficiency and purity of particle separation is equal to 100%. Fig. 24 demonstrates a view of particle separation with and without applying an electric field at Re = 100. The separation of 10-μm particles (blue particles) from 15- and 17-μm particles (yellow and red particles, respectively) is shown due to inertial force. By applying a voltage of 100 V to the microelectrodes, the complete separation of 15- and 17-μm particles is achieved. The results can be used to perform experimental investigations to isolate biological cells such as blood cells and cancer ones. By adjusting the voltage, the amount of dielectrophoretic force required to separate the cells can be provided.

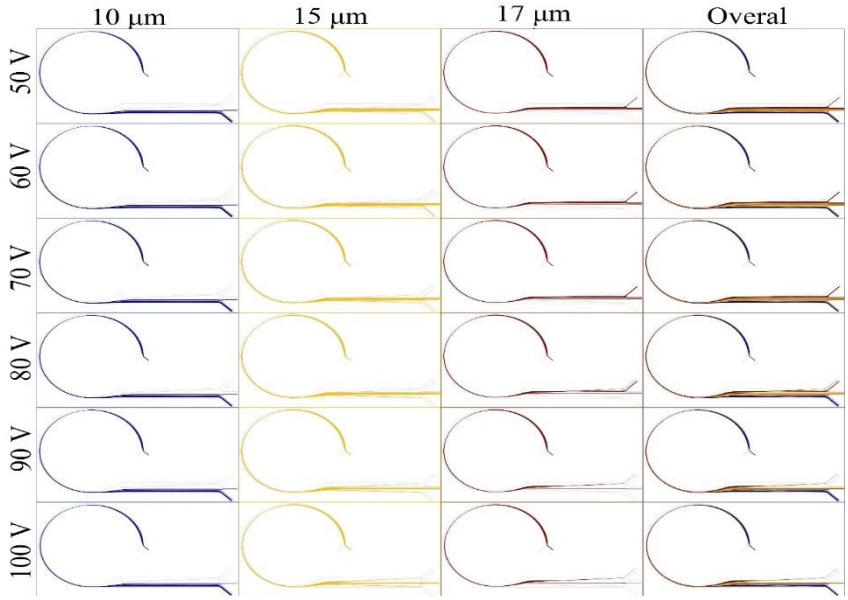

Fig. 18: Particle trajectories for different values of the voltage applied to the electrodes at Re = 100

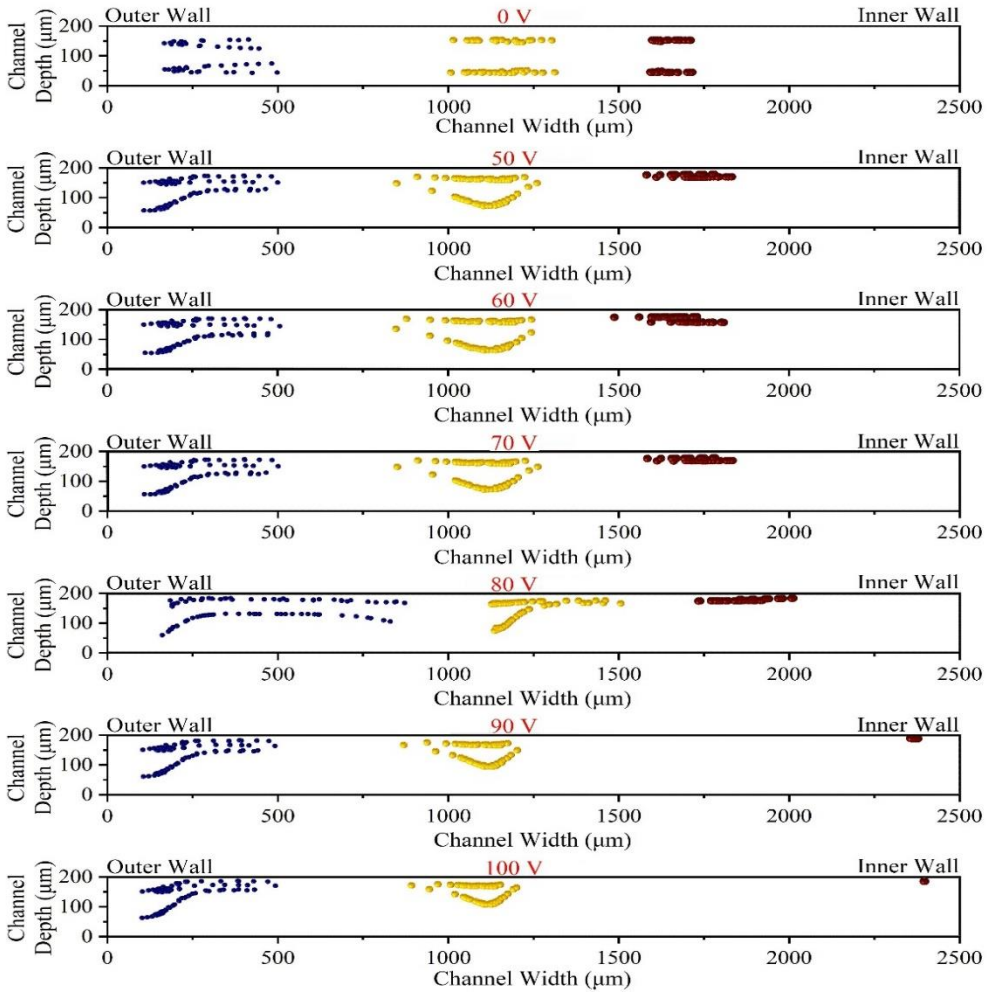

Fig. 19: Transverse location of particles at the channel outlet by applying an electric field at Re = 100

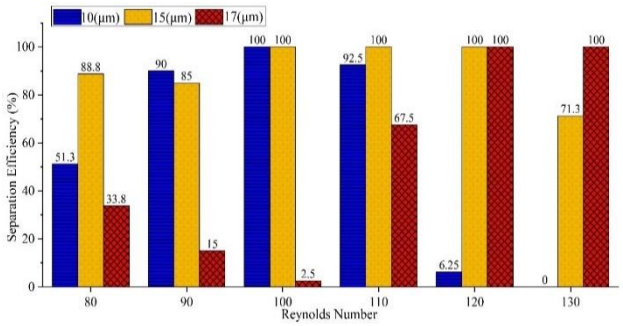

Fig. 20: The efficiency of particle separation without applying the electric field for different Reynolds numbers

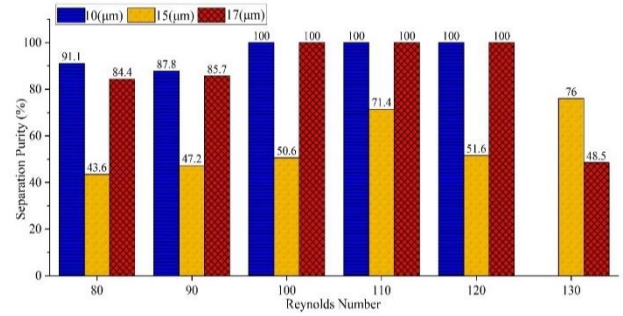

Fig. 21: Purity of particle separation without applying electric field for different Reynolds numbers

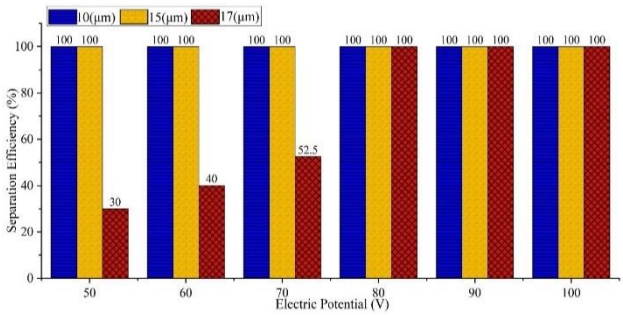

Fig. 22: The efficiency of particle separation by applying an electric field at Re = 100

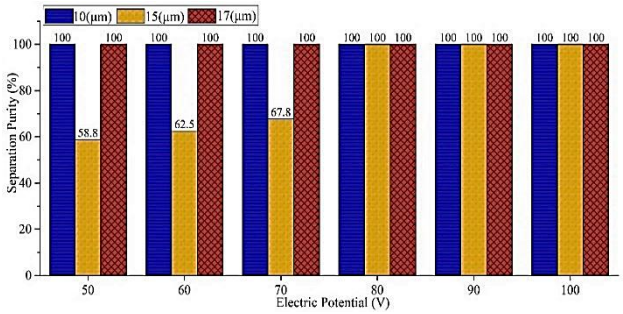

Fig. 23: Purity of particle separation by applying an electric field at Re = 100

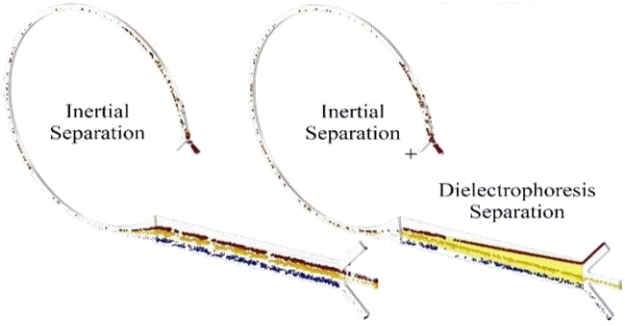

Fig. 24: The separation of particles with (right) and without applying an electric field (left) at Re = 100

Received : Jul. 15, 2022 ; Accepted : Dec. 05, 2022

REFERENCES

[1] Bayareh M., Ashani M.N., and Usefian A., Active and Passive Micromixers: A Comprehensive Review, *Chemical Engineering and Processing-Process Intensification*, **147**: 107771 (2020).

[2] Bayareh M., An Updated Review on Particle Separation in Passive Microfluidic Devices, *Chemical Engineering and Processing-Process Intensification*, **153**: 107984 (2020).

[3] Ashani M.N., Bayareh M., Ghasemi B., Acoustofluidic Separation of Microparticles: A Numerical Study, *Iranian Journal of Chemistry and Chemical Engineering (IJCCE)*, **41(9):** 3064-3074 (2022)

[4] Bhagat A.A.S., et al., Inertial Microfluidics for Sheath-Less High-Throughput Flow Cytometry, *Biomedical microdevices*, **12(2)**: 187-195 (2010).

[5] Li M., et al., A Review of Microfabrication Techniques and Dielectrophoretic Microdevices for Particle Manipulation and Separation, *Journal of Physics D: Applied Physics*, **47(6)**: 063001 (2014).

[6] Chiriac E., Avram M., Balan C., Manipulation of Particles Using Dielectrophoresis in a Microchannel, *Sceience and Technology*, **24(2)**: 213-221 (2021).

[7] Chiu Y.-Y., Huang C.K., Lu Y.W., Enhancement of Microfluidic Particle Separation Using Cross-Flow Filters with Hydrodynamic Focusing, *Biomicrofluidics*, **10(1)**: 011906 (2016).

[8] Tran T.S., et al., Open Channel Deterministic Lateral Displacement for Particle and Cell Sorting, *Lab. on a Chip*, **17(21)**: 3592-3600 (2017).

[9] Bhagat A.A.S., Kuntaegowdanahalli S.S., Papautsky I., Continuous Particle Separation in Spiral Microchannels Using Dean Flows and Differential Migration, *Lab. on a Chip*, **8(11)**: 1906-1914 (2008).

[10] Doh I., Cho Y.H., A Continuous Cell Separation Chip Using Hydrodynamic Dielectrophoresis (DEP) Process, *Sensors and Actuators A: Physical*, **121(1)**: 59-65 (2005).

[11] Shiriny A., Bayareh M., On Magnetophoretic Separation of Blood Cells Using Halbach Array of Magnets, *Meccanica*, **55(10)**: 1903-1916 (2020).

[12] Chen Y., et al., High-Throughput Acoustic Separation of Platelets from Whole Blood, *Lab. on a Chip*, **16(18)**: 3466-3472 (2016).

[13] Neuman K.C., Nagy A., Single-Molecule Force Spectroscopy: Optical Tweezers, Magnetic Tweezers and Atomic Force Microscopy, *Nature Methods*, **5(6)**: 491-505 (2008).

[14] Adekanmbi E.O., Srivastava S.K., Dielectrophoretic Applications for Disease Diagnostics Using lab-on-a-chip Platforms, *Lab. on a Chip*, **16(12)**: 2148-2167 (2016).

[15] Çağlayan Z., Demircan Yalçın Y., Külah H., A Prominent Cell Manipulation Technique in BioMEMS: Dielectrophoresis, *Micromachines*, **11(11)**: 990 (2020).

[16] Martel J.M., Toner M., Particle Focusing in Curved Microfluidic Channels, *Scientific Reports*, **3(1)**: 1-8 (2013).

[17] Shiriny A., Bayareh M., Inertial Focusing of CTCs in a Novel Spiral Microchannel, *Chemical Engineering Science*, **229**: 116102 (2020).

[18] Shiriny A., Bayareh M., Nadooshan A.A., Combination of Inertial Focusing and Magnetoporetic Separation in a Novel Microdevice, *Korean Journal of Chemical Engineering*, **38(8)**: 1686-1702 (2021).

[19] Pommer M.S., et al., Dielectrophoretic Separation of Platelets from Diluted Whole Blood in Microfluidic Channels, *Electrophoresis*, **29(6)**: 1213-1218 (2008).

[20] Piacentini N., et al., Separation of Platelets from other Blood Cells in Continuous-Flow by Dielectrophoresis Field-Flow-Fractionation, *Biomicrofluidics*, **5(3)**: 034122 (2011).

[21] Xing X., et al., Label-Free Enumeration of Colorectal Cancer Cells from Lymphocytes Performed at a High Cell-Loading Density by Using Interdigitated Ring-Array Microelectrodes, *Biosensors and Bioelectronics*, **61**: 434-442 (2014).

[22] Kumar C.L., et al., Computational Microfluidic Channel for Separation of Escherichia Coli from Blood-Cells, *CMC Comput. Mater. Contin*, **67**: 1369-1384 (2021).

[23] Buyong M.R., et al., A Tapered Aluminium Microelectrode Array for Improvement of Dielectrophoresis-Based Particle Manipulation, *Sensors*, **15(5)**: 10973-10990 (2015).

[24] Segre G., Silberberg A.J.N., Radial Particle Displacements in Poiseuille Flow of Suspensions. *Nature*, **189**: 209-210 (1961).

[25] Di Carlo D., et al., Continuous Inertial Focusing, Ordering, and Separation of Particles in Microchannels, *Proceedings of the National Academy of Sciences*, **104(48)**: 18892-18897 (2007).

[26] Hou H.W., et al., Isolation and Retrieval of Circulating Tumor Cells Using Centrifugal Forces, *Scientific Reports*, **3**: 1259 (2013).

[27] Zhang J., et al., Fundamentals and Applications of Inertial Microfluidics: A Review, *Lab. on a Chip*, **16(1)**: 10-34 (2016).

[28] okawara S., Street D., Ogawa K., Numerical Study on Development of Particle Concentration Profiles in a Curved Microchannel, *Chemical Engineering Science*, **61(11)**: 3714-3724 (2006).

[29] Demircan Yalcin Y., Luttge R., 3D-Electrode Integrated Microsieve Structure as a Rapid and Cost-Effective Single Neuron Detector, *Journal of Vacuum Science & Technology B, Nanotechnology and Microelectronics: Materials, Processing, Measurement, and Phenomena*, **38(6)**: 063202 (2020).

[30] Adekanmbi E.O., Giduthuri A.T., Srivastava S.K., Dielectric Characterization and Separation Optimization of Infiltrating Ductal Adenocarcinoma via Insulator-Dielectrophoresis, *Micromachines*, **11(4)**: 340 (2020).

[31] Lin Y.-Y., Lo Y.-J., Lei U., Measurement of the Imaginary Part of the Clausius-Mossotti Factor of Particle/Cell via Dual Frequency Electrorotation. *Micromachines*, **11(3)**: 329 (2020).

[32] Chen Q., Yuan Y.J., A Review of Polystyrene Bead Manipulation by Dielectrophoresis, *RSC Advances*, **9(9)**: 4963-4981 (2019).

[33] Thanormsridetchai A., et al., Focusing and Sorting of Multiple-Sized Beads and Cells Using Low-Aspect-Ratio Spiral Microchannels, *Journal of Mechanical Science and Technology*, **31(11)**: 5397-5405 (2017).